Automated site-specific tip preparation method for atom probe tomography using script-controlled FIB/SEM

Jun Uzuhashi*, Tadakatsu Ohkubo, and Kazuhiro Hono
National Institute for Materials Science, Tsukuba, 305-0047, Japan
**Corresponding author. E-mail: UZUHASHI.Jun@nims.go.jp*

Keywords: APT; atom probe tomography, FIB; focused ion beam, SEM: scanning electron microscopy, automation

Abstract

The automatization of the atom probe tomography (APT) tip preparation using a focused ion beam (FIB) with a scanning electron microscopy (SEM) dual-beam system will certainly contribute to systematic APT research with higher throughput and reliability. While our previous work established a method to prepare tips with a specified tip curvature and taper angle automatically by using script-controlled FIB/SEM, the technique has been expanded to automated "site-specific" tip preparation in the current work. The improved procedure can automatically detect not only the tip shape but also the interface position in the tip, thus, the new function allows for control of the tip apex position, in other words, automated "site-specific" tip preparations are possible. The details of the automation procedure and some experimental demonstrations, *i.e.,* Pt cap on Si, InGaN-based MQWs, and *p-n* junction of GaAs, are presented.

Introduction

Atom probe tomography (APT) has the unique ability to visualize the 3D atomic distribution in materials and devices (Miller, 2000; Gault et al., 2012; Cerezo et al., 1988; Blavette, 1993). The technique has a sub-nanometer spatial resolution and single-atom detectability; therefore, it has become a powerful tool for atomistic microstructural characterization. However, it requires a sharp needle-like specimen (tip) so that a high electric field can be generated at the specimen surface. Earlier, APT tips were prepared using electropolishing; however, the development of a tip preparation method using a focused ion beam (FIB) with scanning electron microscopy (SEM) system enabled site-specific APT analysis of broad ranges of materials possible (Larson et al., 1999; Miller et al., 2005; Sazey et al., 2007; Miller et al., 2007; Hono et al., 2011; Sasaki et al., 2022; McCarroll et al., 2022; Rodenkirchen et al., 2022). However, the tip shapes, such as the radius of the apex angle, prepared by FIB/SEM vary depending on the operator's skills. While the latest commercial APT instruments allow strict control of analysis conditions, the variations in tip shapes still strongly influence the volume of analysis and mass resolution of APT (Cerezo et al., 2007; Arnoldi et al., 2012; Uzuhashi et al., 2023). These previous studies have reported that APT measurement in laser pulsing mode causes a mass tail, and the tip shape influences the magnitude of the mass tail, *e.g.,* mass resolution. Therefore, it has been strongly desired to develop a method to automatically prepare tips with a specified shape reproducibly.

In recent years, script-controlled FIB/SEM systems have been commercialized, and several examples of automated TEM specimen fabrications have been demonstrated (Volkenandt et al., 2017; Leer et al., 2018; Dutka1 et al., 2019). In contrast to the conventional method that depends on the skill of the FIB/SEM operator and the experiment, the automated TEM specimen preparation results in reproducibility, high throughput, and statistical research work. Since it is known that the tip shape for APT analysis in the laser pulsing mode strongly affects the mass resolution (Cerezo et al., 2007; Arnoldi et al., 2012), we developed a method to fabricate tips in a specified shape automatically using a script-controlled FIB/SEM system (Uzuhashi et al., 2023). In our previous work, we systematically evaluated the tip shape influence on the APT data quality and have revealed that the tip shape is also one of the essential parameters in laser pulsing mode not only analysis condition (Uzuhashi et al., 2023). The current work has extended the automated tip preparation technique to “site-specific”. Here we report the procedure of the site-specific automated tip preparation method and some examples of the applications to APT analysis of multi-layer semiconductor devices.

Experimental Methods

A FIB/SEM system, *Thermo Fisher Scientific* Helios 5UX, was used to prepare APT tips automatically. The instrument is equipped with an "AutoScript 4" that can control the FIB/SEM system with a Python-based scripting language. In addition to the standard Python 3.6 library, the following open-source Python libraries were used in our scripting; ConfigObj 5.0.6 for reading and writing of configuration files, NumPy 1.15.4 for the mathematical algorithm, tifffile 2020.9.3 for reading image and metadata, Pillow 5.2.0 for opening and saving images, scipy 1.2.1 and openCV 4.0.1 for image processing, and the further information can be found in our previous paper (Uzuhashi et al., 2023). APT measurements were carried out using *CAMECA* LEAP5000XS with 500 kHz UV laser pulsing mode at a base temperature of 30 K.

The Si needle with a Pt cap was used as the target material, for a simplified system. In addition, the InGaN-based multi-quantum wells (MQWs) and the *p-n* junction of GaAs semiconductors were selected to demonstrate practical APT examples. The structure of InGaN-based MQWs is as GaN top

layer (150 nm) / [InGaN (3 nm) / GaN (10nm)]$_4$ / GaN substrate. The GaAs sample consists of *p*-type GaAs doped with Zn (1000 nm) and *n*-type GaAs doped with Si (1000 nm), the details of which can be found in the previous paper (Sasaki et al., 2014).

Experimental Results and Discussion

Figure 1 shows a schematic of an automated APT specimen fabrication method using a script-controlled FIB/SEM system. When the Python-based program is executed on the FIB/SEM machine, the FIB process starts to fabricate a tip. The tip shape is monitored by SEM imaging, and the result gives feedback to the FIB milling process. The uniqueness of this work is that the automation process is controlled not only by the pre-defined FIB fabrication process, *i.e.,* milling pattern and fabrication time, but also by monitoring the tip shape through the SEM image. This procedure leads to a more reproducible tip fabrication with a specified shape.

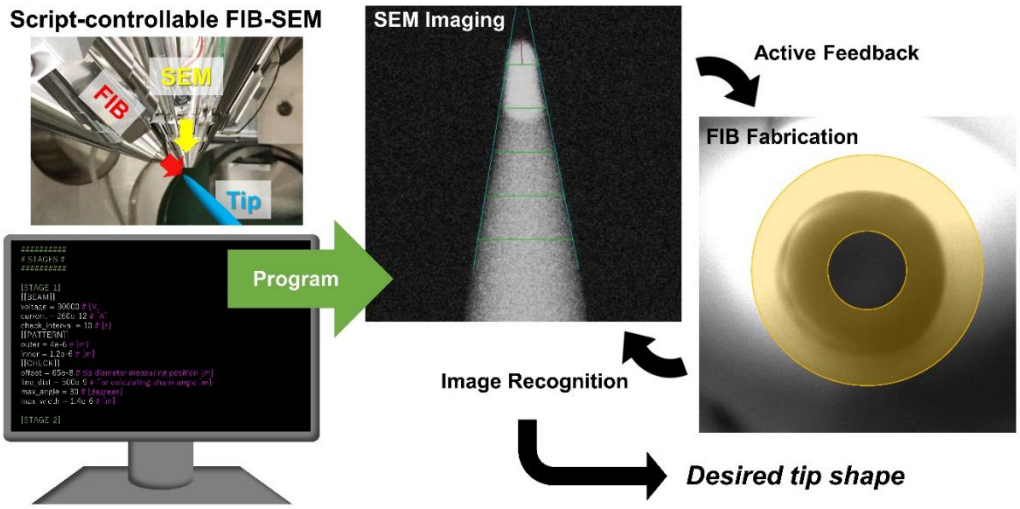

Figure 1. Schematic of an automated tip fabrication using a script-controllable FIB/SEM system. Run the Python-based program on a script-controllable FIB/SEM, then repeat tip shape monitoring using an SEM image and active feedback FIB fabrication until the tip has the desired shape.

The tip shape is defined by the radius of curvature and the shank angle as shown in **Fig. 2(a)**. Details of the tip shape definition are described in our previous paper (Uzuhashi et al., 2023), and the boundary extraction method called "canny edge detection" was applied to the SEM image to monitor the shape (Basu, 2002). A new function for monitoring the interface position has been implemented in this work as shown in **Fig. 2(b)**. A back-scattered electron (BSE) image in the immersion mode with a through-the-lens detector (TLD) is applied here instead of a secondary electron (SE) image because the BSE image shows the z contrast which enables the distinction of the interface. The tip shown in **Fig. 2(b)** is the Si needle with a Pt cap observed by the TLD-BSE detector. The position of the interface can be identified based on the contrast change. The intensity is minimized in a vacuum region, and is brightest at the Pt cap and intermediate (gray) at the Si needle in the TLD-BSE image. It should be noted that the position of the interface in the core region of the tip should be higher than the interface observed in the SEM image by $r_{interface} \times \tan(90 - \theta)$ nm as shown in **Fig. 2(b)**, where θ is the coincidence angle of FIB and SEM beam. For the *Thermo Fischer Scientific* Helios 5UX, θ is 52 degrees. This allows the program to automatically monitor the tip shape and find the interface position.

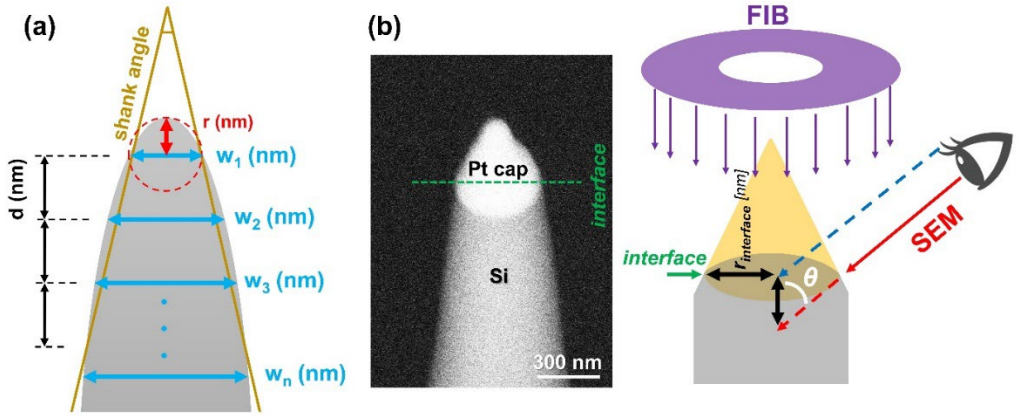

Figure 2. Definition of tip shape. (a) Schematic of the tip shape defined by the radius of curvature and the shank angle. (b) A typical TLD-BSE image of the Pt-capped Si needle during the FIB sharpening process. The coincidence angle θ of FIB and SEM should be considered to determine the interface position.

In our previous study, we prepared tips with different shapes, and their influence on the APT results was studied (Uzuhashi et al., 2023). In this work, the tip shape is fixed since the aim of this work was the addition of a "site-specific" tip preparation function to the previously reported automated tip preparation method. The pre-defined FIB fabrication conditions and the tip shape parameters are shown in **Table 1**. In general, the contrast of the interface in an SEM image becomes weaker if the tip diameter becomes smaller; therefore, we set up the program so that the position of the interface can be registered at the end of the 30 keV FIB process. By using the registered interface position, the program can precisely control the position of the tip apex in the low keV cleaning process. In addition, it allows the program to set the negative values acceptable not only positive values since the minus value is also necessary if the protective cap needs to be removed.

Step	FIB		Donut-shaped Mask		Tip Shape Parameters		
	Voltage	Current	Outer (nm)	Inner (nm)	Radius (nm)	Shank angle (degrees)	Interface Position (nm)
1	30 keV	0.26 nA	4000	1200	＜700	＜30	-
2			3000	700	＜400	＜25	-
3				200	＜100	＜15	# The position registered.
4	5 keV	63 pA	1500	0	＜75	＜15	＜ # Target Position

Table 1. Pre-defined FIB fabrication conditions and the tip shape parameters for the automatic tip preparation. Note that the target interface position can be set from positive values to negative ones according to the APT purpose.

Figure 3 shows the demonstration of site-specific automated tip preparation by monitoring the tip radius of curvature, the shank angle, and the remaining Pt cap height. Here, the target Pt height was intentionally set as negative 400 nm to show how our program monitors the tip shape. **Fig. 3(a)** shows the tip radius, shank angle, and the remaining Pt height as a function of FIB fabrication duration. The program monitors these values in real-time, which gives active feedback to FIB fabrication. Since the height of the remaining Pt cap is also monitored, the program can stop the

FIB fabrication according to the target height. The TLD-BSE images at the locations marked with red color in Fig. 3(a) as (b)~(d) are shown in **Fig. 3(b)~(d)**. The Pt can be observed as the brighter contrast due to the z contrast in the BSE image. Before the low keV cleaning step, the interface position is pre-registered in **Fig. 3(b)**. The tips with Pt height of positive 54 nm and negative 250 nm are shown in **Fig. 3(c) and (d)**. The tip radius, shank angle, and remaining Pt cap height can be successfully monitored in **Fig. 3**. The endpoint values of the low keV FIB process should be set according to the purpose of the APT analysis. This procedure automatically terminates the FIB milling at the desired tip apex position regardless of the target materials in principle, because the termination is decided only by the SEM image recognition. Here, it should be noted that the precision of tip monitoring would be improved if the SEM images were obtained more frequently with higher SEM resolutions; however, it may cause the tip drift problem due to the longer processing time, *i.e.,* there is a tradeoff between the precision of monitoring the tip and the tip drift problem.

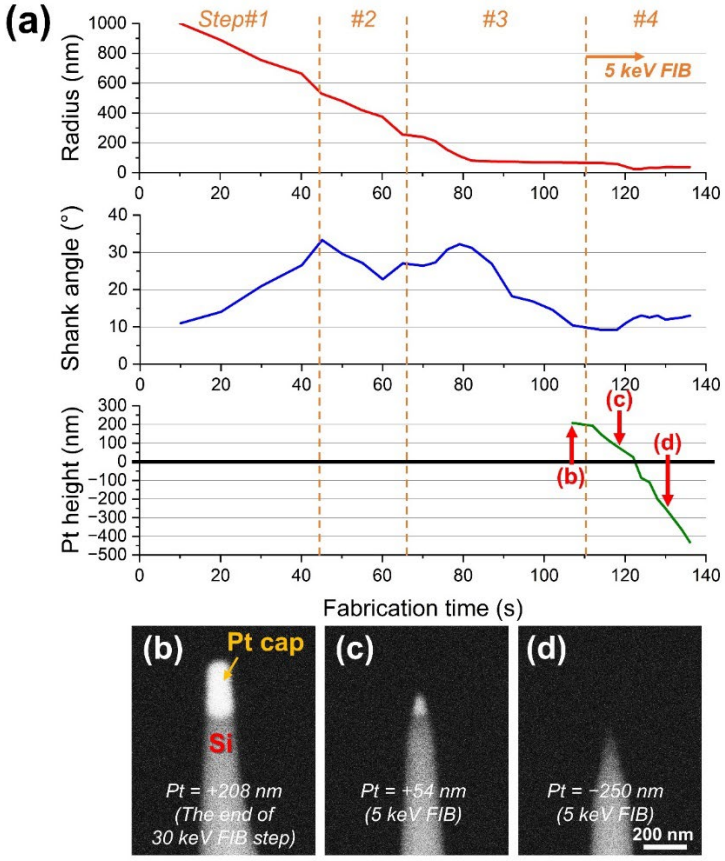

Figure 3. Demonstration of how the automated tip preparation program works. (a) Monitored tip radius, shank angle, and the remained Pt height as a function of FIB fabrication time. Here, the target Pt height was set as - 400 nm to show how the program works. (b) The Si tip at the end of 30 keV (step 4 in Table 1). (c) The tip with 54 nm Pt cap remaining. (c) The Si tip after the Pt protection is completely removed by the low keV FIB cleaning.

The next sample for the automatic "site-specific" tip preparation was InGaN/GaN MQWs, and the schematic structure is shown in **Fig. 4(a)**. The Ni cap has a significant role in minimizing FIB-induced damage (Thompson et al., 2006). The FIB accelerating voltage dependence of the FIB-induced damage can be found in previous studies (Giannuzzi et al., 2005; Giannuzzi, 2006; Mayer et al., 2007). The Ni cap was intentionally kept at ~50 nm during the final low-voltage FIB process to minimize the

FIB-induced damage. **Fig. 4(c)** shows the 3D atom map obtained from the automatically prepared tip (**Fig. 4(b)**). As seen, the program successfully demonstrated that the Ni protection was maintained on the InGaN/GaN MQW sample. Thus, maintaining the protective cap can minimize the FIB damage in the sample.

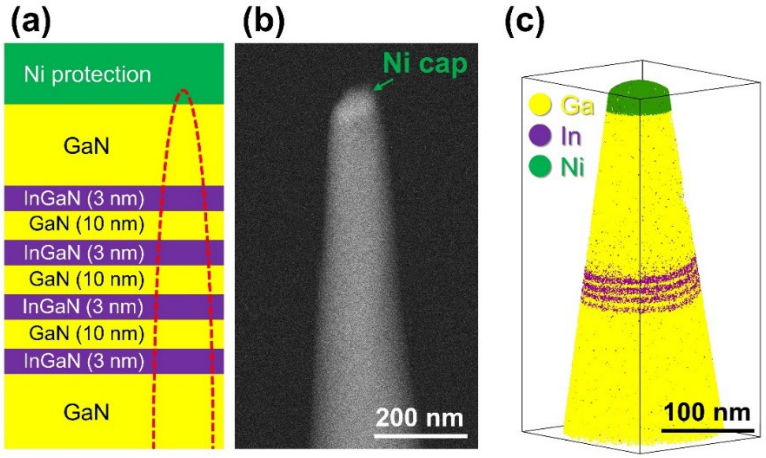

Figure 4. The demonstration of the automatic "site-specific" tip preparation from the InGaN-based MQWs with the Ni protection cap. (a) The schematic of the sample structure. (b) The SEM image of the prepared tip in which Ni was intentionally kept at ~50 nm. (c) The obtained 3D atom map from the tip.

The *p-n* junction of GaAs semiconductor was also demonstrated in this work. As shown in **Fig. 5(a)**, the total 1000 nm Zn-doped *p*-GaAs is formed on the Si-doped *n*-GaAs. The dopant concentration changes in the 200 nm step (Sasaki et al., 2014). Here, we focus on the *p-n* junction of GaAs. In this case, the region of interest is 1000 nm deeper from the sample surface. Therefore, the tip apex must be located near the *p-n* junction; however, there is no contrast change at the *p-n* junction in the SEM image as shown in **Fig. 5 (b)**. As mentioned in the Pt/Si needle case, the negative values are also acceptable as the target value of the tip apex position. In this way, the tip from the ~700 nm depth from the sample surface was automatically prepared as shown in **Fig. 5(b)**. **Figure 5(c)** shows the result of the APT analysis, and the 3D atom map from the region of interest was successfully obtained.

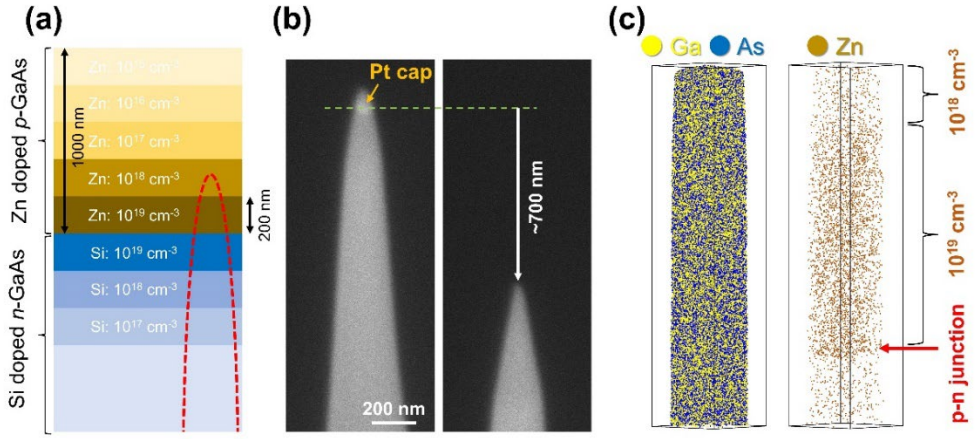

Figure 5. The automatically prepared tip from a *p-n* junction of GaAs. (a) The schematic of the sample structure. The *p-n* junction is located at a depth of 1,000 nm from the surface. (b) The final tip with the top ~700 nm was removed. (c) The obtained 3D atom map of Ga, As, and Zn.

As shown in **Fig. 3, 4, and 5**, the "site-specific" APT tips have been successfully demonstrated by the automation program in this work. Although the throughput of tip preparation by the current

automated program is almost the same as the manual process by skilled FIB-SEM operators, the importance of automation is reproducible tip preparation being able to improve the reliability of APT data. On the other hand, the samples demonstrated in this paper have relatively simple structures, and the interface is located perfectly vertically along the tip. Practical samples would have much more complicated structures, *i.e.,* the interface is located diagonally, the contrast changes may be much weaker, or grain boundaries are difficult to detect by SEM contrast. Here, although there may be others, the following issues are considered concerns for the current automation. (1) Since the appearance of contrast in SEM images varies depending on the target material, it is necessary to select the appropriate SEM detector and the observing conditions. (2) There is a concern that this program may not work properly if the target interface consists of materials with significantly different FIB milling rates. (3) We may need to consider the specimen drift if the FIB milling rate of the target material is significantly slow, in other words, fabrication time becomes longer. (4) In some cases of preparing the APT tip from the different types of interfaces, *i.e.,* vertical interface, an additional automated function to find the optimal position of the FIB fabrication pattern is also required. From these concerns, further improvements and studies are needed as future issues. However, the procedure and demonstrations of the automatic technique shown in our previous report (Uzuhashi et al., 2023) and this paper will strongly contribute to the statistical and reliable APT analysis.

Conclusion

In summary, we have established an automated method to prepare "site-specific" APT tips with tip shape control using a script-controlled FIB/SEM system. The demonstration by using Pt capped Si needle, InGaN-based MQWs, and *p-n* junction of GaAs are shown in this paper. Nowadays, "automation laboratory" is one of the major trends in materials research since it provides benefits of reproducibility, high-quality data acquisition, higher yields, and data-driven research. Thus, the development of an automated APT tip preparation technique will contribute the systematic APT research, reproducible APT analysis, and higher throughput. This script can be available upon a reasonable request at UZUHASHI.Jun@nims.go.jp (J. Uzuhashi).

Acknowledgments

The authors thank Smart Solutions Inc. for supporting the writing of the scripting for the FIB/SEM system, and Kyoko Suzuki for her technical support. In addition, we would thank Sony Semiconductor Solutions Corporation for providing the InGaN/GaN MQWs, and Furukawa Electric Inc. for the *p-n* junction of GaAs.

References

1. Miller, M.K., Atom Probe Tomography: Analysis at the Atomic Level, Kluwer Academic, New York, 2000. https://doi.org/10.1007/978-1-4615-4281-0
2. Gault, B., Moody, M.P, Cairney, J.M., Ringer, S.P., Atom Probe Microscopy, Springer Series in Materials Science, 2012. https://doi.org/10.1007/978-1-4614-3436-8
3. Cerezo, A., Godfrey, T.J., and Smith, G.D.W., Application of a position-sensitive detector to atom probe microanalysis, Rev. Sci. Instrum. **59**, 862 (1988). https://doi.org/10.1063/1.1139794
4. Blavette, D., Deconihout, B., Bostel, A., Sarrau, J.M., Bouet, M., and Menand, A., The tomographic atom probe: A quantitative three-dimensional nanoanalytical instrument on an atomic scale, Rev. Sci. Instrum. **64** (1993) 2911. https://doi.org/10.1063/1.1144382

5. Larson, D.J., Foord, D.T., Petford-Long, A.K., Liew, H., Blamire, M.G., Cerezo, A., Smith, G.D.W., Field-ion specimen preparation using focused ion-beam milling, Ultramicroscopy **79** (1999), 287. https://doi.org/10.1016/S0304-3991(99)00055-8
6. Miller, M.K., Russell, K.F., and Thompson, G.B., Strategies for fabricating atom probe specimens with a dual beam FIB, Ultramicroscopy **102** (2005), 287. https://doi.org/10.1016/j.ultramic.2004.10.011
7. Saxey, D.W., Cairney, J. M., McGrouther, D., Honma, T., and Ringer, S.P., In situ site-specific specimen preparation for atom probe tomography, Ultramicroscopy **107** (2007), 756. https://doi.org/10.1016/j.ultramic.2006.06.008
8. Miller, M.K. and Russell, K.F., Atom probe specimen preparation with a dual beam SEM/FIB miller, Ultramicroscopy **107** (2007), 761. https://doi.org/10.1016/j.ultramic.2007.02.023
9. Hono, K., Ohkubo, T., Chen, Y.M., Kodzuka, M., Oh-ishi, K., Sepehri-Amin, H., Li, F., Kinno, T., Tomiya, S., and Kanitani, Y., Broadening the applications of the atom probe technique by ultraviolet femtosecond laser, Ultramicroscopy **111** (2011), 576-583. https://doi.org/10.1016/j.ultramic.2010.11.020
10. Sasaki, T.T., Sepehri-Amin, H., Uzuhashi, J., Ohkubo, T., and Hono, K.. Complementary and correlative (S)TEM/APT analysis of functional and structural alloys. MRS Bulletin **47** (2022), 688-695. https://doi.org/10.1557/s43577-022-00374-7
11. McCarroll, I.E., Daly, L., White, L.F., Cairney, J.M., Atom probe tomography and correlative microscopy: Key techniques for future planetary science studies. MRS Bulletin **47** (2022), 696-705. https://doi.org/10.1557/s43577-022-00375-6
12. Rodenkirchen, C., Appleton, M., Ryan, M.P., Pedrazzini, S., A review on atom probe and correlative microscopy studies of corrosion in nickel-based superalloys. MRS Bulletin **47** (2022), 706-717. https://doi.org/10.1557/s43577-022-00366-7
13. Cerezo, A., Clifton, P.H., Gomberg, A., Smith, G.D.W., Aspects of the performance of a femtosecond laser-pulsed 3-dimensional atom probe, Ultramicroscopy **107** (2007), 720-725. https://doi.org/10.1016/j.ultramic.2007.02.025
14. Arnoldi, L., Vella, A., Houard, J., Deconihout, B., Antenna effect in laser assisted atom probe tomography: How the field emitter aspect ratio can enhance atomic scale imaging, Appl. Phys. Lett. **101** (2012), 153101. https://doi.org/10.1063/1.4757884
15. Uzuhashi, J., Ohkubo, T., and Hono, K., Development of automated tip preparation for atom probe tomography by using script-controlled FIB-SEM, Ultramicroscopy **247** (2023), 113704. https://doi.org/10.1016/j.ultramic.2023.113704
16. Volkenandt, T., Pérez-Willard, F., Rauscher, M., Anger, P.M., Towards Automatic Lamella Thinning Using Live Thickness Measurements and Smart End-Point Detection, Microscopy and Microanalysis 23 (2017), 304-305. https://doi.org/10.1017/S1431927617002203
17. Leer, B.V., Geurts, R., Scharfschwerdt, R., Cheng, H., Li, L., and Imlau, R., New Workflows Broaden Access to S/TEM Analysis and Increase Productivity, Microsc. Today 26 (2018), 18–25. https://doi.org/10.1017/S1551929517001195
18. Dutka1, M., and Prokhodtseva, A., AutoTEM 5 – Fully Automated TEM Sample Preparation for Materials Science, Microscopy and Microanalysis 25 (2019), 554-555. https://doi.org/10.1017/S1431927619003507
19. Sasaki, H., Otomo, S., Minato, R., Yamamoto, K., and Hirayama, T., Direct observation of dopant distribution in GaAs compound semiconductors using phase-shifting electron holography and

Lorentz microscopy, Microscopy **63** (2014), 235–241. https://doi.org/10.1093/jmicro/dfu008
20. Basu, M., Gaussian-based edge-detection methods-a survey, IEEE Trans. Syst. Man Cybern. Part C Appl. Rev., **32** (2002), 252-260. https://doi.org/10.1109/TSMCC.2002.804448
21. Thompson, K., Gorman, B., Larson, D.J., Leer, B.V., Hong, L., Minimization of Ga Induced FIB Damage Using Low Energy Clean-up, Microscopy and Microanalysis **12** (2006), 1736–1737. https://doi.org/10.1017/S1431927606065457
22. Giannuzzi, L.A., Geurts, R., and Ringnalda, J., 2 keV Ga+ FIB Milling for Reducing Amorphous Damage in Silicon, Microscopy and Microanalysis **11** (2005), 828-829. https://doi.org/10.1017/S1431927605507797
23. Giannuzzi, L.A., Reducing FIB Damage Using Low Energy Ions, Microscopy and Microanalysis **12** (2006), 1260-1261. https://doi.org/10.1017/S1431927606065469
24. Mayer, J., Giannuzzi, L.A., Kamino, T., Michael, J., TEM sample preparation and FIB-induced damage, MRS Bulletin **32** (2007), 400-407. https://doi.org/10.1557/mrs2007.63